Radiometric Techniques for Emissivity and Temperature Measurements for Industrial Applications

(Article begins on next page)

25 November 2024

Radiometric techniques for emissivity and temperature measurements for industrial applications

E M Vuelban[1,4], F. Girard[2], M. Battuello[2], P. Nemeček[3], M. Maniur[3], P. Pavlásek[3], T. Paans[1]

[1] VSL, Thijsseweg 11, 2629 JA, Delft, the Netherlands

[2] Istituto Nazionale di Ricerca Metrologica, Strada delle Cacce, 91 - 10135 Torino, Italy

[3] Slovenský Metrologický Ústav, Karloveská 63, 842 55 Bratislava 4, Slovakia

[4] To whom correspondence should be addressed. E-mail: evuelban@vsl.nl

Abstract

Radiometric techniques for temperature measurements are indispensable in industrial applications particularly when the use of contact thermometers is hard or impossible to realize. We present here the principles and realizations of some new and extended radiometric techniques for measuring the emissivity and temperature of an object. Using the described techniques, the emissivity and temperature of an Inconel 600 sample at high temperatures in laboratory condition were determined. The validation of the temperature measurement of the same sample in a simulated industrial condition is also presented.

1 Introduction

Radiometric methods for temperature measurement are noncontact and noninvasive techniques, which can be advantageous in various industrial applications where the use of contact methods (e.g., thermocouples, resistance thermometers, etc) is not permissible due to harsh or extreme measurement conditions [1-2]. However, there are two major issues associated with the use of such radiometric techniques for temperature measurements. The first is the unknown emissivity of the object, which is necessary to determine subsequently the object's true surface temperature. The second issue is the influence of background radiation from nearby objects and the emission from and absorption by the environment. These issues significantly influence the radiation reaching the detector and the resulting temperature reading.

Radiation thermometers (RT) measure the radiation (radiance) emitted by the object and by using known fundamental physical formula (e.g., Planck's law of radiation or Stefan-Boltzmann's law), the corresponding surface temperature of the object associated with the emitted radiation can be determined. For a perfect emitter such as a blackbody, the Planck's distribution for the spectral intensity of radiation emitted at temperature T is given by [1],

$$L_{\lambda,b}(\lambda,T) = \frac{c_1}{\lambda^5 (\exp(c_2/\lambda T) - 1)} \tag{1}$$

where c_1 and c_2 are the radiation constants ($c_1 = 1.1911 \times 10^{-16}$ W·m^{-2}·sr^{-1} and $c_2 = 1.4388 \times 10^{-2}$ m·K), and λ is the radiation wavelength. For a real surface, however, the radiation emitted is smaller than that of the blackbody at the same temperature due to its intrinsic emissive (absorptive) characteristic. The spectral emissivity of a non-ideal emitter is defined as the ratio of the spectral intensity of radiation emitted by a real surface, $L_{\lambda,r}(\lambda,T)$, to that emitted by a blackbody, $L_{\lambda,b}(\lambda,T)$, at the same temperature and spectral condition,

$$\varepsilon_\lambda = \frac{L_{\lambda,r}(\lambda,T)}{L_{\lambda,b}(\lambda,T)} \tag{2}$$

In real measurement situation, all radiation entering into the aperture of the RT is being detected by the instrument. Apart from the radiation from object itself, the detected radiation includes the irradiation from the surroundings that is reflected by the target surface, target surface irradiation that is reflected by the surroundings and then the target itself, and atmospheric scattering and absorption from water vapor, various gases and dust particles. For an opaque surface (with accompanying diffused irradiation from a large surrounding at a given temperature T_{sur}), the measured radiation intensity can be expressed as,

$$L_{\lambda,m}(\lambda,T) = \varepsilon_\lambda L_{\lambda,b}(\lambda,T) + (1 - \varepsilon_\lambda) L_{\lambda,b}(\lambda,T_{sur}) \tag{3}$$

where $(1-\varepsilon_\lambda)$ is the spectral reflectivity of the target surface, which is the fraction of the irradiation from the surroundings at T_{sur}.

In this article, we describe the principles and experimental realizations of various radiometric techniques for determining the emissivity and temperature of an object. These techniques include the "virtual source" method (VSM) for surface emissivity determination, thermal imager for large area surface temperature measurement, and the UV-multiwavength radiation thermometry (MWT) approach for simultaneous temperature and emissivity measurements. Further, the results from the validation of the temperature measurements in a simulated industrial condition, using an *Inconel* 600 sample placed inside an industrial furnace and heated at high temperatures (600 °C and 900 °C), are presented. The results from the temperature measurements performed in laboratory conditions using a reference RT and the MWT setup is qualitatively compared with the temperature measurements performed in a simulated industrial condition using a transfer RT.

2 Virtual-source Method for Emissivity Measurement

Though radiation thermometry techniques have undergone significant improvements in the last decade, the precise determination of the emissivity of an unknown material remains one of the many challenging issues which influences the reliability of such radiometric methods. In this section, we present the principle of the "virtual source" method for determining the emissivity of a sample without the need to consider the sample temperature itself.

Figure 1 shows the model used for emissivity measurements using the virtual source method. The model system consists of the following components: sample S with a unknown emissivity ε and temperature T, shutter C with an aperture of r_1 radius which is placed in the position L_1 from the sample, point detector D in the position L_0 from the shutter C, a planar mirror M with reflectance ρ and with an outer radius of R_{mo} and aperture radius of R_{mi}. The shutter, mirror and detector are aligned with respect to the radiation source axis. The space surrounding the sample, together with the shutter, mirror and detector, is assumed to have a temperature T_0 and has the characteristics of a blackbody.

When we assume that the sample radiation has a Lambertian character, the radiation intensity is then $M_s = \varepsilon \sigma T_s^4$, where σ is the Stefan-Boltzman constant. The radiant flux generated by the sample or reflected from the sample is the measured signal. The radiation reflected from the sample is in the line of sight of the detector and has an area of A_d. When the mirror is in the position L_2 the aperture radius R_{mi} is greater than the radius of the line of sight of the detector which is determined by the position L_0 and by the radius r_1 of the aperture C. The radiant flux from the sample consists mainly of two source contributions: a) radiation

directly coming from the source, and b) radiation from the virtual source (radiation reflected from the mirror). The radiation flux contribution from the source itself can be expressed as,

$$\Phi_S = \varepsilon\sigma T^4 A_d \tag{4}$$

while the radiation from the virtual source can be expressed as,

$$\Phi_{S0} = \varepsilon(1-\varepsilon)\rho\sigma T^4 G_{VS-d} A_{VS} \tag{5}$$

where A_{VS} is the surface of the virtual source and G_{VS-d} is the so-called geometrical configuration factor (GCF) [3]. For diffusion sources, the GCF is defined as,

$$G_{S\text{-}T} = \frac{1}{A_S} \int\limits_{A_S} \int\limits_{A_T} \frac{\cos\beta_S \cos\beta_T}{\pi L^2} dA_T dA_S \tag{6}$$

where A_S and A_T represent the areas of the radiation source and the irradiated surface, respectively. The β_S and β_T are the angles between the normal to the elementary surface dA_S, dA_T and the connection of these elementary surfaces with the length L. The GCF is a non-dimensional coefficient which expresses the quotient of the energy from the source emitted onto the target and the overall energy generated by the source and emitted to the surrounding space.

The flow Φ_{S0} generates a secondary source of radiance which irradiates the surface A_d with an intensity of $\Phi_{S0}A_d^{-1}$. The same source (after a double reflection from the mirror and from the surface of the source) creates a tertiary source with a flow Φ_{S1} which is expressed as

$$\Phi_{S1} = \Phi_{S0}A_d^{-1}A_d G_{d-VS}\rho^2 A_{VS}^{-1}A_{VS}G_{VS-d}(1-\varepsilon)^2 \tag{7}$$

When the flow reciprocity

$$A_d G_{d-VS} = A_{VS}G_{VS-d} \tag{8}$$

is applied, we can express the tertiary source flow as

$$\Phi_{S1} = \Phi_{S0}(1-\varepsilon)^2 \rho^2 A_d^{-1} A_{VS}^{-1} A_{VS}^2 G_{VS-d}^2 = \Phi_{S0}F \tag{9}$$

$$F = \left[(1-\varepsilon)\rho A_{VS}G_{VS-d}\frac{1}{\pi R_{VS}R_d} \right]^2 \tag{10}$$

where F expresses the irradiation of the source by itself through the mirror. The result of this repeated reflection from the mirror is the radiant flux Φ_{VS}.

$$\Phi_{VS} = \Phi_{S0} + \Phi_{S0}F + \Phi_{S0}F^2 + ...\Phi_{S0}F^n.... = \Phi_{S0}\left(1 + F + F^2... + F^n...\right) = \Phi_{S0}\frac{1}{1-F} \tag{11}$$

For the mentioned geometry of the virtual source and from the GCF point-of-view, the source is divided into three annuli (figure 1). The radii of the first and the third annulus (R_1 and R_2) are determined by the points A, A´ and the radii R_3 and R_4 of the other annuli are determined by the points B and B´. These annuli are the virtual sources of radiation from which the flow on the surface A_d is limited by the outer and the inner edges of the mirror (figure 1). Therefore the calculation of GCF is possible according to Eq. (6) or according to the Stokes theorem [3]. The flow from annulus A to annulus B with radii R_2 and R_3 is expressed as a difference of flows from circular sources with the relevant radii. The GCF for the flow from circular source

with radius r_S that irradiates the target with radius r_T in the position L can be expressed by the following equation:

$$G(r_s, r_T, L) = \frac{1}{2}\left\{ \left[1 + \frac{1 + \left(r_T/L\right)^2}{\left(r_s/L\right)^2}\right] - \sqrt{\left[1 + \frac{1 + \left(r_T/L\right)^2}{\left(r_s/L\right)^2}\right]^2 - 4\frac{\left(r_T/L\right)^2}{\left(r_s/L\right)^2}} \right\} \tag{12}$$

The overall flow from the surface A_d is a sum of all the flows from each individual parts of the virtual source and it is given by the radii R_1, R_2, and R_3 which are placed in the position $2L_2$. This overall flow is expressed as,

$$\Phi_{CVS} = \Phi_S + \left[\Phi_{VS1}(R_1, R_2, 2L_2) + \Phi_{VS2}(R_3, R_2, 2L_2) + \Phi_{VS3}(R_2, R_3, 2L_2)\right] \tag{13}$$

Implicitly the above equation for the overall flow contains the calculation of the GCF. In Eq. (13), the expression in the square brackets represents the flow component which is dependent on position of the mirror. This flow component can be expressed as,

$$\Phi_{VS}(L_2) = \varepsilon(1-\varepsilon)\rho\sigma T^4 \left[G_{VS1-d}A_{VS1}F_{VS1} + G_{VS2-d}A_{VS2}F_{VS2} + G_{VS3-d}A_{VS3}F_{VS3}\right] \tag{14}$$

A similar mathematical expression can be used to express the radiation source from the surrounding space at temperature T_0. The radiation from the environment which is reflected by the surface A_d can be divided into two parts. The first part consists of the radiation coming from the environment directly onto the mentioned surface,

$$\Phi_{01}(L_2) = (1-\varepsilon)\sigma T_0^4 A_d \left(1 - G_{z-d}\frac{A_z}{A_d}\right) \tag{15}$$

where A_z ($A_z = \pi R_z^2$) is the mirror's surface area and G_{z-d} is the GCF for the radiation flux generated from the mirror to the surface A_d. The last component enclosed in the bracket in Eq. (15) represents the shading of the sample from the environment. The second part consists of the radiation from the environment but now the radiation irradiates the sample and through the reflections from the mirror it gets on the surface A_d. This part of radiation flux that the sample is exposed to, is in the terms of geometry confirmation factor of surfaces and the correlation factor F (which expresses the multiplicity of reflections for the self-irradiation of the sample) is identical with the expression for the radiation coming from the sample, Eq. (14). The equation of the second part of the radiation from the environment reflected by the surface A_d is expressed as

$$\Phi_{02}(L_2) = (1-\varepsilon)^2\rho\sigma T_0^4 \left[G_{VS1-d}A_{VS1}F_{VS1} + G_{VS2-d}A_{VS2}F_{VS2} + G_{VS3-d}A_{VS3}F_{VS3}\right]\cdot\left(1 - G_{z-VS}\frac{A_z}{A_{VS}}\right) \tag{16}$$

In Eq. (16), the last component in the bracket represents the shading of the radiation from the environment, just like in Eq. (15). The flows Φ_{VS}, Φ_{01}, Φ_{02} are flow components which are dependent on the mirror position but are additive components to Φ_s, which is independent of position. If there is no mirror in the model, then the flow which generates the signal is given by the equation,

$$\Phi_{S0} = \sigma A_d \left[\varepsilon T^4 + (1-\varepsilon)T_0^4\right] = \Phi_s + (1-\varepsilon)\sigma A_d T_0^4 \tag{17}$$

As a characteristic quantity for the emissivity determination, we took the flow differences from the measurements done with the mirror and with the standardized flow with mirror and without the mirror reduced by the flow from the modulator $\Phi_m = A_d\sigma T_m^4$. When we assume that the temperatures of the

surrounding space and of the modulator are equal, then the ratio between the generated signals and radiation fluxes can be expressed by

$$\frac{U(L_2) - U_s}{U_s} = \frac{\Phi_{VS} + \left[\Phi_{01} + \Phi_{02} - (1-\varepsilon)\sigma A_d T_0^4\right]}{\varepsilon \sigma A_d \left(T^4 - T_0^4\right)}$$

(18)

Normalizing the signal to the form of a radiation flux or signal U_s we are able to omit the dependence of the flow, Φ_{VS}, on the temperature. This will also cause the reduction of the component $\varepsilon.(\varepsilon-1)$ to the following one $(\varepsilon-1)$. The residual correction component of the dominant component Φ_{VS} is in the following form $(1-T_0^4/T^4)^{-1}$. Its determination at high temperatures can be done by simply estimating its value which is based on the estimation of the temperature T. Similarly, we can think in the same way by the flow which is expressed in the square brackets from the Eq. (18). This component expresses the flow from the environment which has been superimposed by the reflection from the sample [3, 4].

3 Large Surface Area Temperature Measurement using Thermal Imager

Thermal imagers measure a much larger area of the sample surface, unlike conventional single-spot RT, and provide a spatial distribution of the surface temperature in the form of an image [5-6]. Similar to single-spot RT, the radiation distribution measured by a thermal imager does not only depend on the temperature of the object but also on its emissivity. The radiation is also highly influenced by various extraneous radiation sources mentioned in section 1, which should be taken into account and properly corrected when performing accurate temperature measurements. Most commercially available thermal imagers have auto-correction capabilities incorporated in the imager´s software. However, the correct values for the object's emissivity, the reflected apparent temperature from the surrounding, the focus distance of the imager, the humidity and temperature of the atmosphere are still being manually inputted into the imager software by the user in order to obtain a reliable temperature reading.

Figure 2 shows a model for temperature measurement using a thermal imager. For a given object temperature T_{obj}, the total radiation power, according to Stefan-Boltzmann's law, received by the TI can be written as [5],

$$W_{tot} = \varepsilon \tau W_o + (1-\varepsilon)\tau W_r + (1-\tau)W_{atm}$$

(19)

where the first term, $\varepsilon\tau W_o$, is the radiative power emanating from the object (with emissivity ε), that traverses the atmosphere having a transmittance τ. The second term, $(1-\varepsilon)\tau W_r$, is the ambient source reflected radiative power, where the term $(1-\varepsilon)$ is the object´s reflectance. The ambient source is assumed to have a reflectance temperature T_r, which is considered to be the same for all emitting surfaces within the hemisphere seen from a point on the object surface. For simplification, the value for the ambient temperature represents an effective temperature of a complex surrounding. The emittance of the surrounding is assumed to be 1, which is a reasonable assumption based on Kirchhoff's law [2]. The last term of the measurement Eq. (19) is the radiative contribution from the atmosphere, $(1-\tau)W_{atm}$. The atmosphere is assumed to have a

temperature T_{atm}. The resulting generated voltage signal corresponding to the radiation from the object can be expressed as

$$V_o = (\varepsilon\tau)^{-1} V_t - (\varepsilon^{-1}-1)V_r - [(\varepsilon\tau)^{-1} - \varepsilon^{-1}]V_{atm} \qquad (20).$$

Equations (19-20) are the general measurement equations used in all forward-looking infrared type thermal imagers [7].

4 Multiwavelength Approach for Simultaneous Temperature and Emissivity Measurements

Multi-wavelength thermometry is essentially based on the measurement of the radiance of a source at several wavelengths and, following some assumptions on the emissivity behaviour of the object, on the derivation of the temperature of the source from these measurements. The approach can be implemented in different constructional ways. In the past, it was common to split or select the incoming radiation by means of optical filters with the consequence that was limited to few and fixed working wavelength bands [8, 9]. Nowadays, the use of linear PDA or CCD array detectors in conjunction with a spectrally-selective device (e.g., a monochromator or a spectrograph) allows realizing devices with a high degree of flexibility both in terms of the numbers and position of the working wavelength bands. However, in practice these advantages are not sufficient to make the multi-wavelength approach reliable for operations in the VIS-NIR (e.g., in the spectral range useful for temperature measurements around 1000 °C or less). Operating in the typical wavelength band of 0.65 μm - 0.95 μm has many negative consequences, particularly the high sensitivity to the measurement noise and to model errors (errors arising from an incorrect assumption of the behaviour of the spectral emissivity). On the other hand, this should not be surprising because the multi-wavelength approach essentially is an extrapolation process towards $\lambda \to 0$ of measurement data obtained in a defined spectral range (as discussed in the next section). At the same time, such considerations also suggest that reducing the extrapolation range should reduce the relevant errors. A simulation process was carried out at which it was confirmed that shortening the operating wavelengths down to 0.35 μm considerably reduce the influence of both the measurement noise and model errors [10]. Errors due to random noise can be reduced by a factor of more than 20 when the emissivity can be modelled with a 2nd order polynomial. The model errors are largely dependent on the equation used in the model and consequently a detailed investigation was carried out with both real materials and some fictitious linear equations. The reduction of the model errors when the measuring system was operated to the 0.35-0.95 μm band was consistent with all equation models. From the initial characterization performed of the set-up, it has been found that the MWT can be operated at temperature as low as 900 °C at wavelengths from 500 nm up. Such a still short wavelength limit is an essential requisite for taking advantage of the UV operation. Such feature turned out to be important because it allows measuring an Inconel 600 sample at 900 °C.

A multi-wavelength thermometer measures the spectral radiances from a source at several wavelengths. The Wien's approximation of the Planck's law (shown in Eq. (1)) can be conveniently used, and is expressed as

$$L_{\lambda,T}(\varepsilon_\lambda) = \varepsilon_\lambda c_1 \lambda^{-5} \exp\left(-\frac{c_2}{\lambda T}\right) \tag{21}$$

where λ is the wavelength, and c_1 and c_2 are the radiation constants presented in section 1, ε_λ is the spectral emissivity and T is the temperature in Kelvin. By extending the case of the two-colour thermometer in which the temperature can be derived simply by taking the ratio of the radiances:

$$R_{1,2} = \frac{L_{\lambda_1}(\varepsilon_{\lambda_1}, T_R)}{L_{\lambda_2}(\varepsilon_{\lambda_2}, T_R)} = \frac{\varepsilon_{\lambda_1} L_{\lambda_1}(T)}{\varepsilon_{\lambda_2} L_{\lambda_2}(T)} \Rightarrow \frac{1}{T_R} = \frac{1}{T} - \frac{\lambda_1 \lambda_2}{c_1(\lambda_2 - \lambda_1)} \ln\left(\frac{\varepsilon_{\lambda_1}}{\varepsilon_{\lambda_2}}\right) \tag{22}$$

provided that the emissivities are the same at both wavelengths, $\varepsilon_{\lambda_1} = \varepsilon_{\lambda_2}$. Similarly, extending this expression to more than two wavelengths, Eq. (21) can be generalized into

$$L_{\lambda_i,T}(\varepsilon_{\lambda_i}) = \varepsilon_{\lambda_i} c_1 \lambda_i^{-5} \exp\left(-\frac{c_2}{\lambda_i T}\right) \tag{23}$$

which is basically a system of N equations with $N+1$ unknowns can be obtained, where $i = 1, \ldots N$ is the number of wavelengths used. By assuming the emissivity to be a function of the wavelength with no more than $N-1$ coefficients, the system of equations will contain no more than N unknowns and consequently can be analytically solved.

A possible approach, suggested by Coates [8], consists in taking the logarithm of the emissivity versus wavelength represented by a polynomial expressed in the form,

$$\ln(\varepsilon_\lambda) = \sum_{j=0}^{j=M} a_j \lambda^j \tag{24}$$

and with a degree $M \leq N - 2$. The spectral radiances can be written down in a straightforward way and consequently all the succeeding calculations are greatly simplified. By combining Eq. (23) and Eq. (24), the following equation can be obtained,

$$Y_i = \frac{c_2}{T} - \lambda_i \sum_{j=0}^{j=M} a_j \lambda_i^j \tag{25}$$

where,

$$Y_i = \lambda_i \left[-\ln L_{\lambda_i,T}(\varepsilon_{\lambda_i}) + \ln(c_1) - 5\ln(\lambda_i)\right] \tag{26}$$

are the measured radiance terms. Consequently, the temperature and the emissivity can be simultaneously derived by solving the system of equations above.

In practice, to search for the value of T in the Eq. (25) corresponds to searching for the value of Y_i when λ tends to zero:

$$\lim_{\lambda \to 0}\left(\frac{c_2}{T} - \lambda_i \sum_{j=0}^{j=M} a_j \lambda_i^j\right) \tag{27}$$

and the Eq. (25) assumes the form:

$$T = \frac{c_2}{Y_i} \tag{28}$$

The full procedure appears to be as an extrapolation process towards $\lim \lambda \to 0$. The system of equations to be solved can be expressed and written in matrix form as:

$$\vec{Y} = \begin{bmatrix} Y_1 \\ Y_2 \\ \dots \\ Y_N \end{bmatrix} = \begin{bmatrix} c_2 & -\lambda_1 & -\lambda_1^2 & \dots & -\lambda_1^{M+1} \\ c_2 & -\lambda_2 & -\lambda_2^2 & \dots & -\lambda_2^{M+1} \\ \dots & \dots & \dots & \dots & \dots \\ c_2 & -\lambda_N & -\lambda_N^2 & \dots & -\lambda_N^{M+1} \end{bmatrix} \times \begin{bmatrix} 1/T \\ a_0 \\ \dots \\ a_M \end{bmatrix} = M \times \vec{A} \tag{29}$$

where $\vec{Y}$ is a N dimensional vector containing the measured data (the radiances at N different wavelengths), M is a matrix whose dimension are $(M + 2) \times N$ and containing the constant terms c_2 and the wavelengths, and $\vec{A}$ is a vector of dimension $M + 2$ containing the unknowns (the temperature and the emissivity coefficients). Finally, the vector $\vec{A}$, normally obtained by means of the least square method, can be expressed as follow:

$$\vec{A} = \left(M^T M \right)^{-1} M^T \vec{Y} \tag{30}$$

5. Experimental Realization

5.1 Virtual Source Method

Fig. 3 shows the schematic and actual realization of the virtual-source measurement set-up with individual components. The tested sample in which the emissivity was determined was *Inconel* 600 plate with dimensions of 100 mm by 100 mm by 1.6 mm. The sample was measured at temperatures of 580 °C, 600 °C and 620 °C. The mirror used in the measurements had a diameter of 50 mm and the aperture in the middle of the mirror had a diameter of 5 mm. The mirror coating has a reflectivity of 0.98 ($\rho = 0.98$). The aperture *IC1* has a diameter of 2 mm and its distances to the detector were as follows: $L_0 = 420$ mm, $L_1 = 315$ mm, $L_3 = 325$ mm, $L_4 = 410$ mm. The value of L_2 is varied between 50 mm to 120 mm. The aperture *IC2* has a slightly larger dimension than IC1 (diameter of 7 mm).

For the measurements of radiation a Bentham DH-PY pyrometer was used which can operate on wavelengths of 1 µm - 50 µm. A chopper (CTX 15) with a frequency of 15 Hz was also used during these measurements. The time constant during the whole measuring procedure was 3s. The *Inconel* 600 plate is securely attached to a ceramic holder with a heating element, which is powered by an electric source with a regulation option. This ensures the high stability of the temperature in the vicinity of the sample. The temperature of the sample was measured to assign the calculated emissivity value to the true sample temperature and determine the change of emissivity with temperature. Further, temperature measurements were done to determine the influence of the change of the reflectivity of the mirror at various temperatures

and make the needed correction. The sample temperature was measured using various thermocouples. One approach was the measurements of temperature by a calibrated type S thermocouple which was put into the enclosed cavity that was between the heater element and the sample. The thermocouple tip position was in contact with the sample. The other method used a commercial type K thermocouple specially designed for the surface temperature measurements. The distance of the mirror from the sample was measured by calibrated scale embedded into the optical bench on which the experimental setup was assembled.

5.2 Multiwavelength Radiation Thermometry Method

Figure 4 shows the major assemblies of the MWT setup for simultaneous temperature and emissivity measurements. The first assembly is the MWT detector, which is based on two devices (a spectrograph Horiba Scientific model MicroHR-Auto and a TE-cooled CCD detector Horiba Sincerity 1024 x 256, coupled together). A detailed technical description of the characteristics of both devices can be found in [9]. Table 1 shows the hardware configuration of the detector assembly used during the temperature and emissivity measurements. The second assembly is the blackbody furnace. A modified commercial LAND calibration source model R1500T equipped with six silicon carbide (SiC) heaters was used as a reference source for deriving the spectral responsivity curve of the MWT. A SiC cavity with 45 mm internal diameter and 95 mm length was constructed. For the measurement comparison, a 15 mm diameter diaphragm was placed at the aperture of the furnace to make the size-of-source effect (SSE) contributions from furnace and sample similar. In these conditions, the calculated effective emissivity of the cavity is greater than 0.998. The radiance temperature of the blackbody cavity was defined with the standard radiation thermometer (SRT), as a reference thermometer which is a primary standard of INRIM. The SRT is based on a Si photodiode (Hamamatsu S2592-03) operated in unbiased mode with a built-in Peltier cooler (allowing the temperature of the detector to be controlled at +10 °C). The SRT is a fixed-focus instrument with a working distance of 675 mm with a minimum target size of 1.5 mm. For the measurement comparison, the spectral configuration based on a filter centred at 950 nm with a FWHM of 70 nm was used and a multi fixed-points calibration scheme was adopted. The thermometer was calibrated at the Zn, Al, Ag and Cu point and the Sakuma-Hattori equation was used to interpolate between the fixed points.

Like in the virtual source method for emissivity determination, the material used to realize the MWT method is *Inconel* 600 (disk with diameter of 16 mm and thickness of 1.6 mm). The sample was mounted onto a heating sample holder a scheme of which is shown in figure 5. This configuration allows a metallic sample of less than 3 mm in thickness to be heated by conduction up to temperature exceeding 900 °C. The surface temperature of the sample is measured in an independent way with the SRT at a wavelength of 950 nm by applying the correction for the spectral emissivity of the sample at the same wavelength of 950 nm. The emissivity has been previously measured at such wavelength and at a temperature of approximately 900 °C by means of a high-temperature integrating sphere reflectometer of the comparison type [11]. The value of

0.929 was found for the spectral emissivity at 950 nm and 900 °C. A complete run of the measurements comprising the following:

a) The temperature T_{ref} of the blackbody reference source is measured with the SRT;

b) The radiance spectra of the blackbody reference source between 500 nm and 950 nm are acquired with the MWT.

c) The surface temperature of the heated *Inconel* 600 sample is measured with the SRT. Such a step is necessary for the successive comparison with the temperature as measured with the MWT.

d) The radiance spectrum of the *Inconel* 600 between 500 nm and 950 nm is acquired with MWT.

e) The response curve of the MWT is derived by dividing the output curve obtained at step b) by the Planck curve at T_{ref}.

f) The radiance spectrum of the *Inconel* 600 is obtained by dividing the output curve at step d) by the response curve of the MWT.

g) The radiance spectrum of *Inconel* 600 is analysed with the multi-wavelength approach as discussed in Section 3. A software (based on VBA) dedicated for the set-up has been developed which calculate the temperature and the coefficients of linear polynomials (from 0th to 2nd order) for the spectral emissivity. Different spectral sub-ranges can be selected.

h) The different elaborations, in terms of both different emissivity model and spectral sub-ranges, are analyzed.

5.3 Facility for Validation of Temperature Measurement in a Simulated Industrial Condition

Figure 6 shows a small-scale industrial furnace (slightly modified to provide a variable aperture), which was used as a facility for the validation of temperature measurements in a simulated industrial condition (e.g., in petrochemical processing). The modified furnace has a maximum operating temperature up to 1300 °C. The furnace is equipped with its own temperature controller. It has inner dimensions of 460mm (W) x 690 mm (D) x 685 mm (H). Various target elements such as plates and tubes can be placed easily inside the furnace for non-contact temperature measurements. For a plate element, the largest dimension which can be placed inside is 440 mm (W) x 300 mm (H) x 15 mm (T). A maximum of three tube elements, having equal dimension of 100 mm (OD) x 10 mm (WT) x 300 mm (H), can be placed inside the furnace at the same time. The plate element inside the furnace can be oriented at an angle with respect to the thermometer line-of-sight. Both the plate and tube elements are provided with separate heating facility in order to achieve various temperature conditions of the target surface and the environment inside the furnace. The plate element has its own calibrated thermocouple clamped onto the surface of the material to measure independently the temperature using contact method. For the tube elements, the calibrated thermocouples are embedded inside the tube wall thickness.

The *Inconel* 600 samples, with dimensions previously stated in sections 5.1 and 5.2, were first thermally treated at 950 °C continuously for about 3 days (at ambient atmosphere) to obtain a stable surface oxide layer. Repeated tests were then performed to ascertain that the oxide layer is already thermally stable at 950 °C before performing the real validation measurements.

Before the samples were sent to other laboratories (SMU for emissivity and INRIM for temperature and emissivity) these were first measured inside the abovementioned facility. After the other laboratories were finished with their respective measurements, the samples were sent back to VSL for re-measurement. For the measurements, the resulting surface temperature of the *Inconel* 600 samples at various temperature conditions between the sample and the furnace, namely $T_{sample} = T_{furnace}$, and $T_{sample} > T_{furnace}$ were investigated. For all the measurements performed, the samples were securely attached to the large heated plate element and were positioned at the center of the plate and the furnace aperture. The nominal temperatures of the samples were set using the temperature controller of the large plate element where the Inconel 600 samples were securely attached. The temperature was monitored using the thermocouple provided for the large heated plate element. When the thermocouple reading is already stable, temperature measurements were then performed, using first the transfer standard RT (single-spot RT from LAND Instruments) and then the uncooled microbolometer TI. The temperature measurements of the sample sent to SMU for emissivity measurements were performed only at setpoint temperatures 580 °C, 600 °C, and 620°C in order to adjust to the limited operating temperature of the virtual source setup (temperature of about 600 °C max). Thus, only the emissivity value at 600 °C can be used to correct for the temperature measurements done using the TI. On the other hand, the MWT set-up can operate only at minimum temperature of around 900 °C. For the temperature measurements at 900 °C, the MWT results are qualitatively compared with the results from the transfer standard RT only, since the TI results cannot be corrected for the correct emissivity.

6. Results and Discussion

6.1 Emissivity Measurement using the Virtual Source Method

The results of the emissivity measurements for the *Inconel* 600 sample are presented in table 2. The measurements were performed at setpoint temperatures of 580 °C, 600 °C, and 620 °C. For each temperature setpoint, five measurement runs were performed. The average emissivity of the *Inconel* 600 sample at 600 °C is 0.85. These values were obtained using a Bentham DH-PY pyrometer, which operates at wavelength range of 1 μm to 50 μm. For the thermal imager ($\lambda = 8$ μm - 14 μm), the measured emissivity is also about 0.85. The overall measurement uncertainty budget for the virtual source method is presented in table 3. The combined measurement uncertainty is about 0.14 (U (k=2)).

6.2 Temperature and Emissivity Measurements using the MWT Approach

Tables 4 and 5 summarize the results obtained from the MWT approach for the simultaneous temperature and emissivity measurements of the *Inconel* 600 sample at setpoint temperatures 880 °C, 900 C and 920 °C. The MWT was used in the spectral range from 500 nm to 950 nm to measure the sample surface at the above mentioned temperatures. The true surface temperature of the sample was measured with a standard radiation thermometer (SRT) at 950 nm. The spectral emissivity of the *Inconel* 600 sample, measured at INRIM with a high temperature integrating sphere reflectometer, was used to correct for the radiance temperature of the radiation thermometer. The MWT was found to measure temperatures in excess of 5.1 °C, 1.2 °C, 1.4 °C at 880 °C, 900 °C, 920 °C respectively, with respect to the SRT. All these results are within the estimated combined standard uncertainty of the measurement, which is about 5.5 °C. For the spectral emissivity (table 5), the data at 900 °C were analyzed at different spectral ranges between 500 nm and 950 nm. An average linear 1st order polynomial fit was derived from these measurement data, which gives the emissivity values between 0.94 and 0.895 at 500 nm and 950 nm, respectively. The value at 950 nm can be compared with that found with the integrating sphere, i.e., 0.929 and the agreement is within the estimated standard uncertainty, i.e., 0.036 (U (k=1)).

6.3 Temperature Measurements in a Simulated Industrial Condition

Table 6 shows the results of the temperature measurements of the *Inconel* 600 sample inside the industrial furnace using a transfer standard RT (T_{SRT}) and the thermal imager (raw temperature T_{raw} and corrected temperature T_{corr}) at 580 °C, 600 °C, and 620 °C. The corresponding temperatures of the furnace were also set at the same setpoint temperatures. The raw data (average of center 3x3 pixels) for the sample temperatures obtained using the thermal imager are corrected for the emissivity ($\varepsilon = 0.85$ at 600 °C) obtained from the virtual source measurements at the same setpoint temperatures mentioned in section 6.1, and using Eq. (19) we obtained an emissivity-corrected temperature, T_{corr}, of the sample as presented in table 6. In deriving the emissivity-corrected temperatures of the *Inconel* 600 sample, the atmospheric transmission is assumed to be quite close to 1. From table 6, it can be seen that the maximum difference between the corrected temperature reading of the TI and the transfer standard RT is about 2 °C, which is within the estimated combined standard uncertainty of measurement (about 3.5 °C at 600 °C).

Table 7 presents the comparison of the large area surface temperature measurements using the TI and individual single-spot measurements at different positions using the transfer standard RT at 600 °C. The

furnace temperatures are set equal to the setpoint temperatures of the *Inconel* 600 sample. Again, using the emissivity value obtained from the virtual source method, the raw temperature data from the TI measurements are corrected for the emissivity ($\varepsilon = 0.85$, $\tau_{atm} = 1$). In table 7, the left and right positions of the transfer RT represent the measurement spots located 1 cm (left or right) from the center position of the sample respectively. The temperature values obtained with TI are the average temperature values inscribed within a circle corresponding to about 4 cm in diameter on the sample surface. It is however very difficult to compare exactly the spot locations where the temperature reading from the transfer standard RT were taken from the temperature distribution obtained with the TI. As an indication, however, the temperature values obtained are within the estimated uncertainty. An obvious drawback with averaging over a much larger surface area is that the resulting surface temperature would not provide a correct surface temperature representation, especially when localized surface temperature extremes can be present.

6.4 Comparison of the Temperature Measurements between VSL and INRIM (SRT and MWT)

To provide a qualitative comparison between the temperature measurements performed in laboratory condition (using a reference RT and the MWT method) and the measurements performed in a simulated industrial condition (using the transfer standard RT), the results from section 6.2 and 6.3 are summarized in table 8. Only a qualitative comparison between the different methods and measurement conditions can be provided due to the lack of an agreed measurement transfer parameter for the sample (apart from the agreed setpoint temperatures) which can strictly be measured by both methods and measurement conditions. This lack of agreed transfer parameter is mainly due to the complexities involved in each measurement set-up. However from table 8, it is apparent that the temperature readings of the SRTs of VSL and INRIM indicate a good agreement (max $\Delta T = 0.85$ °C). This qualitative comparison provides an indication of the reliability of measuring the surface temperature of *Inconel* 600 sample at different locations and at different conditions. The results from the MWT temperature measurements presented in table 8 also show good agreement with the VSL's transfer standard RT. The difference between the average temperature of the VSL's SRT and the INRIM's MWT is within the uncertainty budget of the MWT measurements ($U_c = 5.5$ °C).

6.5 Sample Stability and Reproducibility of Temperature Measurements

As mentioned in section 5.3, the *Inconel* 600 samples were measured first at VSL before these were sent to the partner institutes for the emissivity and temperature measurements. After the partner institutes were finished with their respective measurements, these samples were sent back to VSL for re-measurement. Table 9 shows the results of the temperature measurements of *Inconel* 600 sample, which was sent to INRIM (before sending and re-measurement after the sample was sent back to VSL). From table 9, the

values obtained for both measurement conditions are quite in good agreement. This indicates that the thermophysical characteristics of the sample were not significantly altered during the MWT measurement. The results from the temperature measurements demonstrate good reproducibility.

7. Conclusions

Various radiometric techniques for emissivity and temperature measurements of *Inconel* 600 samples are presented. From the virtual source method, the emissivity of Inconel at 600 °C, was determined to be 0.85, with a total combined measurement uncertainty of 0.14 at k=2. This determined emissivity value at 600 °C was used to correct for the temperature reading obtained with a TI measuring the same Inconel 600 sample inside an industrial furnace at the same temperature setpoint. The resulting corrected temperature values from the TI are in good agreement with the transfer standard RT ($\Delta T_{max} = 1.7$ °C). Comparing the temperature measurements of the same Inconel 600 sample using the MWT and reference RT in laboratory condition and the transfer RT in a simulated industrial condition, the results also indicated good agreement ($\Delta T_{max} = 4.4$ °C). Thus, the results presented demonstrate that the described methods can be reliably used to determine the correct emissivity and temperature of an unknown sample.

References

1. DeWitt DP and Nutter GD (ed.) 1988 *Theory and Practice of Radiation Thermometry* (New York: John Wiley) pp 1-17

2. Zhang ZM and Lee BJ 2010 Theory of Thermal Radiation and Radiative Properties In: Zhang ZM, Tsai BK and Machin G, editors *Radiometric Temperature Measurement, I. Fundamentals* (Oxford: Academic Press)

3. Siegel R and Howell JR 1972 *Thermal Radiation Heat Transfer* (New York: McGraw-Hill Book Co) p 632

4. Michalski L, Eckersdorf K, Kucharski J and McGhee J 2001 *Temperature measurement* 2nd edition (West Sussex, UK: John Wiley) p 501

5. Kruse PW 2001 *Uncooled Thermal Imaging Arrays, Systems, and Applications* (Bellingham, Washington: SPIE) pp 1-10

6. Vollmer M and Mollmann KP 2010 *Infrared Thermal Imaging: Fundamentals, Research and Applications* (Weinheim, Germany: Wiley-VCH) pp 14-50, 73-137

7. FLIR User's Manual, FLIR R&D software suite 3.1.

8. Coates PB 1981 *Metrologia* **17** 103-109

9. Girard F and Battuello M 2013 *Report on the prototype design of a UV multi-wavelength high-temperature measurement system* (*INRIM Report*, EMRP HiTeMS Project)

10. Girard F, Battuello M and Florio M 2014 *Int J Thermophys* : Online First DOI 10.1007/s10765-014-1678-1

11. Battuello M and Ricolfi T 1989 *High Temperatures. High Pressures*. 21.3 303-309

Table 1 The settings configuration of WMT used during the simultaneous temperature and emissivity measurement of *Inconel* 600 sample.

Parameter	Setting(s)
Input optics (pinhole camera lens)	f-number =100
Standard working distance (WD)	690 mm, (for measuring the sample at 880 °C, WD =520 mm)
Input slit width	0.1 mm
Nominal target shape (WxH)	8.5 mm x 2.4 mm
Grating pitch	150 rows/mm (ruled, with blaze at 500 nm)
Spectrograph center wavelength	500 nm
CCD detector gain	High Sensitivity
exposure times	5 s, 10 s and 20 s (specific measurements, with reference source at 960 °C, have been performed with exposure time of 4.3 s)

Table 2 Measured emissivity values for *Inconel* 600 at different setpoint temperatures using the virtual source method.

Measurement run	$t_s{}^a = 580\ °C$ ε	$t_s{}^a = 600\ °C$ ε	$t_s{}^a = 620\ °C$ ε
1	0.82	0.85	0.85
2	0.81	0.86	0.92
3	0.86	0.79	0.82
4	0.85	0.85	0.78
5	0.89	0.90	0.75
average	0.85	0.85	0.82
std	0.03	0.04	0.07

[a] t_s is the nominal temperature value of the *Inconel* 600 sample (°C)

Table 3 Measurement uncertainty budget for the virtual source method.

Source of uncertainty	Standard Uncertainty	Distribution	Contribution to the standard uncertainty
Emissivity uncertainty (type A)	0.04	Normal (Gaussian)	0.01
Reproducibility	0.03	Uniform	0.02
Sample temperature uncertainty	0.06	Uniform	0.03
Sample temperature distribution	0.10	Uniform	0.06
		combined uncertainty U(k=2)	**0.14**

Source of uncertainty | Standard Uncertainty | Distribution | Contribution to the standard uncertainty

Table 4 Temperature measurements using the multiwavelength thermometry method.

| Measurement run | $t_s = 880\,°C$ | | $t_s = 900\,°C$ | | $t_s = 920\,°C$ | |
	SRT (°C)	MWT (°C)	SRT (°C)	MWT (°C)	SRT (°C)	MWT (°C)
1	882.3	887.4	900.6	905.1	920.5	924
2	882.5	890.7	901	903.5	921.1	922.1
3	880.6	883.5	901.8	905.1	921.4	920
4	881.4	886.8	902.4	901.3	922.4	925
5	881.7	885.5	902.8	899.6	922.8	923
average	881.7	886.8	901.7	902.9	921.6	922.8
std.	0.8	2.7	0.9	2.4	0.9	1.9

Table 5 Derived spectral emissivity of the *Inconel* 600 sample at 900 °C from the MWT method.

Wavelength (nm)	*Emissivity, ε*
500	0.940
550	0.935
600	0.930
650	0.925
700	0.920
750	0.915
800	0.910
850	0.905
900	0.900
950	0.895

Table 6 Temperature measurements of the Inconel 600 sample placed inside the industrial furnace using a single-spot transfer RT (T_{SRT}) and thermal imager (raw temperature T_{raw} and corrected temperature T_{corr}).

Measurement run	$t_s = 580\,°C$			$t_s = 600\,°C$			$t_s = 620\,°C$		
	T_{SRT} (°C)	Traw (°C)	Tcorr (°C)	T_{SRT} (°C)	Traw (°C)	Tcorr (°C)	T_{SRT} (°C)	Traw (°C)	Tcorr (°C)
1	582.4	543.6	583.4	603.0	560.5	601.5	623.0	580.8	623.3
2	582.2	543.6	583.4	604.0	560.6	601.6	623.0	580.9	623.4
3	582.4	543.5	583.3	602.9	560.5	601.5	623.4	581.1	623.6
4	582.4	543.2	583.0	603.7	560.8	601.9	623.4	581.3	623.8
5	582.3	543.3	583.0	602.9	560.7	601.7	622.0	580.9	623.4
average	582.3	543.4	583.2	603.3	560.6	601.6	622.9	581.0	623.5
std	0.1	0.2	0.2	0.5	0.1	0.2	0.5	0.2	0.2

Table 7 Comparison of large area surface measurement with single-spot measurements at 600 °C.

Measurement run	SRT			Thermal Imager	
	left	center	right	Traw	Tcorr
1	603.7	603.0	603.8	559.8	600.6
2	602.9	604.0	602.9	559.7	600.4
3	603.8	602.9	604.1	559.7	600.4
4	602.9	603.7	602.9	559.4	600.1
5	603.3	602.9	603.8	559.4	600.1
average	603.4	603.3	603.5	559.6	600.3
std	0.4	0.5	0.6	0.2	0.2

Table 8 Temperature measurement comparisons using various radiometric methods at different conditions.

Measurement run	$t_s = 880\,°C$			$t_s = 900\,°C$			$t_s = 920\,°C$		
	VSL SRT (°C)	INRIM SRT (°C)	INRIM MWT (°C)	VSL SRT (°C)	INRIM SRT (°C)	INRIM MWT (°C)	VSL SRT (°C)	INRIM SRT (°C)	INRIM MWT (°C)
1	882.8	882.3	887.4	902.3	900.6	905.1	922.8	920.5	924
2	881.8	882.5	890.7	901.4	901	903.5	922.8	921.1	922.1
3	882.8	880.6	883.5	902.7	901.8	905.1	922.8	921.4	920
4	882.8	881.4	886.8	901.7	902.4	901.3	922.6	922.4	925
5	881.8	881.7	885.5	902.3	902.8	899.6	921.6	922.8	923
average	882.4	881.7	886.8	902.1	901.7	902.9	922.5	921.6	922.8
std	0.5	0.8	2.7	0.5	0.9	2.4	0.5	0.9	1.9

Table 9 Temperature measurements of the *Inconel* 600 sample (sent to INRIM) before sending and re-measurement thereafter using a transfer RT

Measurement run	$t_S = 880\,°C$ Before (°C)	After (°C)	$t_S = 900°C$ Before (°C)	After (°C)	$t_S = 920\,°C$ Before (°C)	After (°C)
1	882.8	881.9	902.3	901.8	922.8	922.9
2	881.8	882.8	901.4	902.2	922.8	923.9
3	882.8	881.8	902.7	902.4	922.8	922.8
4	882.8	881.8	901.7	901.9	922.6	922.9
5	881.8	882.8	902.3	902.9	921.6	923.9
average	882.4	882.2	902.1	902.2	922.5	923.3
std	0.5	0.5	0.5	0.4	0.5	0.6

Figure Captions
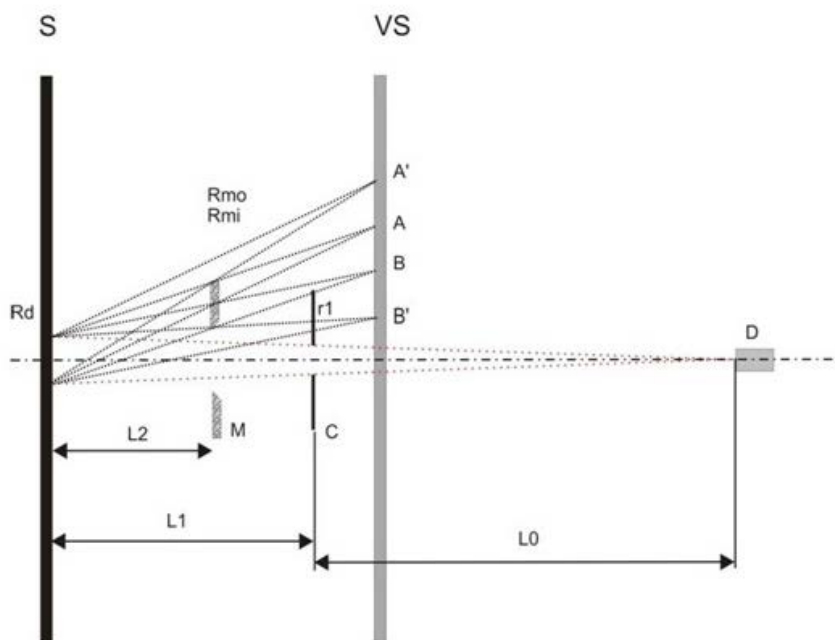
Fig. 1 Model of the virtual source method

Fig. 2 Model for temperature measurement using a thermal imager (adapted from [7]).

Fig. 3 Schematic of experimental realization of the virtual-source method of measuring emissivity

Fig.4 Multiwavelength set-up for temperature and emissivity measurements

Fig. 5 Schematic of the heating sample holder for the *Inconel* 600 artefact

Fig. 6 Facility used for the validation of temperature measurements in a simulated industrial condition, a) small-scale industrial furnace with b) fully opened aperture and c) variable-size aperture
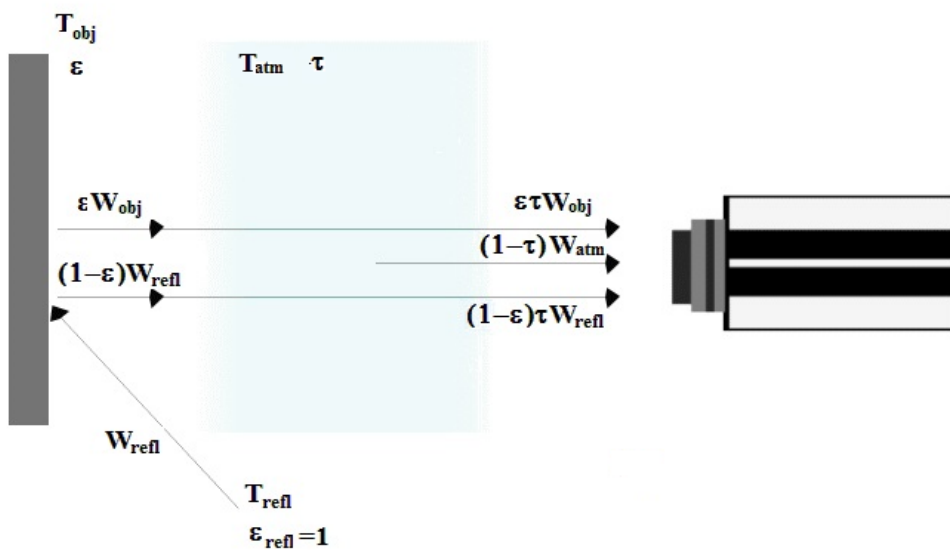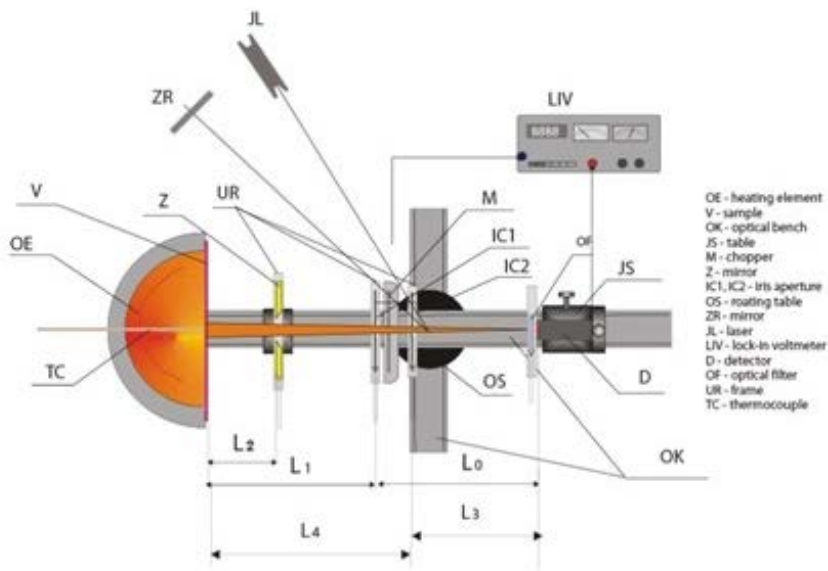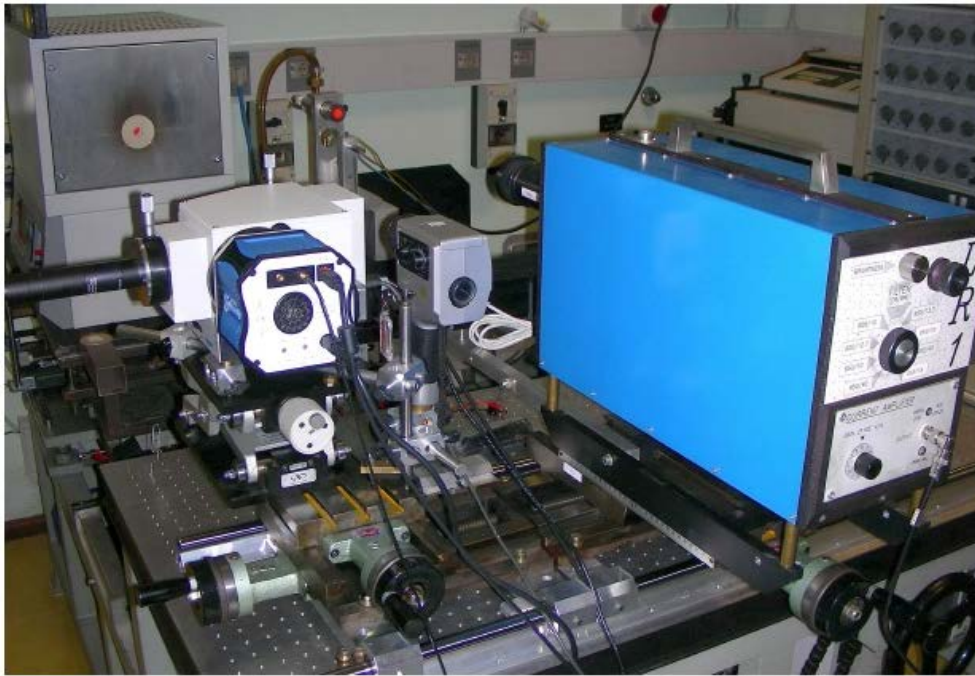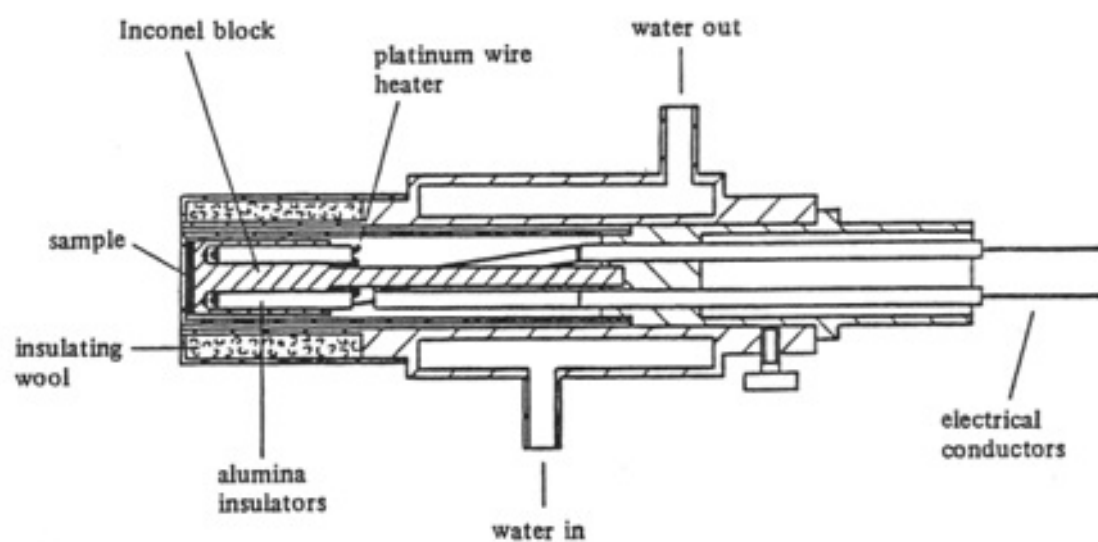
Fig. 1

Fig. 2

OE - heating element
V - sample
OK - optical bench
JS - table
M - chopper
Z - mirror
IC1, IC2 - iris aperture
OS - rotating table
ZR - mirror
JL - laser
LIV - lock-in voltmeter
D - detector
OF - optical filter
UR - frame
TC - thermocouple

Fig. 3

Fig. 4

Fig.5

Fig.6